Analysis of Electrically Large Antennas using Fast Physical Optics

Oscar Borries[1,2], Hans-Henrik Viskum[2], Peter Meincke[2],
Erik Jørgensen[2], Per Christian Hansen[1], Carsten H. Schmidt[3]
[1]Technical University of Denmark, DTU Compute, Kgs. Lyngby, Denmark, {opbo,pcha}@dtu.dk
[2]TICRA, Læderstræde 34, DK-1201 Copenhagen, Denmark, {ob,hhv,pme,ej}@ticra.com
[3]Airbus Defence & Space, Munich, Germany, carsten.schmidt@astrium.eads.net

***Abstract*—The design of electrically large antennas can be a significant challenge for computational electromagnetics (CEM) tools, particularly during the final stages of the design process where there are strict requirements for the accuracy. In the present paper, we consider the use of a newly developed accelerated Physical Optics (Fast-PO) and show that this approach allows for a timely and accurate solution of realistic designs. Several examples, ranging from canonical tests of the scaling of the method against the wavelength to real-life applications, illustrate the performance of the approach in practice.**

I. Introduction

Computational electromagnetics (CEM) tools have long since established themselves as a vital part of the design approach for modern antennas. A range of approaches exist for modelling the behaviour of antennas of varying size and complexity, and choosing the right tool for the job is very critical in order to achieve an acceptable runtime while maintaining an adequate accuracy.

When considering electrically large reflector antennas, for applications such as space or telecommunications, achieving both low runtimes and low error levels typically involve the use of Physical Optics (PO). PO is an asymptotic method where the surface current density is approximated as if the surface at the point of observation is replaced by its tangent plane. This approximation becomes increasingly accurate with increasing frequency f, but unfortunately the computation time of PO behaves as $\mathcal{O}(f^4)$. In other words, for electrically very large antennas, even PO can become prohibitively slow in practice.

The time-consuming part of PO is the evaluation of the radiated field from a surface current distribution, in which each observation point requires evaluation of a two-dimensional integral. Thus, speeding up PO requires speeding up the evaluation of fields from current distributions. The speedup of this subtask is also beneficial in other methods, such as Radar Cross Section (RCS) evaluation and Method of Moments (MoM), where it is used both to evaluate the right-hand side and to find the field radiated by the computed currents.

Several research groups have considered the acceleration of these tasks. An early version is the fast far-field approximation (FaFFA) [1] and its multi-level variants, which represent the behaviour of the field outside a sphere of radius $2D^2/\lambda$ as a sum of plane waves, one from each subgroup of current points, where D is the diameter of the group. Since the Rayleigh distance $2D^2/\lambda$ is only an approximate value of the distance at which the far-field behaviour of the current distribution begins, the error level is not controllable when applying FaFFA.

An alternative was presented in [2] and further expanded in [3], [4], [5]. This algorithm, which we will refer to as Fast-PO, uses interpolation as the main tool to allow the computation of radiated fields on a reduced grid and then interpolate to the requested observation points. Since direct interpolation would not yield significant savings, the interpolation is performed on a phase-compensated field, which is much easier to interpolate, and the original phase is then restored. The accuracy is mainly controlled by increasing the order of the polynomial interpolant. However, choosing the parameters to achieve a specified accuracy is not straight-forward for a general scatterer. Further, achieving the accuracy levels required for some reflector antenna applications is difficult using polynomial interpolants.

In the present paper, we briefly review the Fast-PO algorithm, highlighting its strengths and weaknesses. Then, we focus on the performance on an improved version when applied to a wide range of test cases.

II. Fast Physical Optics

PO constitutes a high-frequency approximation to the induced surface current density $\boldsymbol{J}_{\mathcal{S}}$ on a perfectly electrically conducting scatterer $\mathcal{S}$ given by

$$\boldsymbol{J}_{\mathcal{S}} = \begin{cases} 2\hat{\boldsymbol{n}} \times \boldsymbol{H}_i & \text{if illuminated} \\ 0 & \text{otherwise} \end{cases} \tag{1}$$

where $\boldsymbol{H}_i$ is the incident magnetic field and $\hat{\boldsymbol{n}}$ is the outward unit normal vector of $\mathcal{S}$. Finding $\boldsymbol{J}_{\mathcal{S}}$ from (1) requires very little work itself, but computing the field from $\boldsymbol{J}_{\mathcal{S}}$, or finding $\boldsymbol{H}_i$ from a general surface current density, requires evaluation of an integral which may involve a significant amount of computational work. In the present context, the main applications are computing the electric far-field from $\boldsymbol{J}_{\mathcal{S}}$ or computing the magnetic near-field from another surface to form $\boldsymbol{H}_i$ in (1). In the following, we consider each of these applications separately, since the involved integrands possess very different properties.

A. Far-field Fast-PO

Computing the electric far-field in the direction (θ, ϕ) from a surface current distribution $\boldsymbol{J}_{\mathcal{S}}$ is done by computing

$$\boldsymbol{E}_{\text{far}}(\theta,\phi) = \frac{jk\eta_0}{4\pi}\hat{\boldsymbol{k}}\times \left[\hat{\boldsymbol{k}} \times \iint \boldsymbol{J}_{\mathcal{S}}(\boldsymbol{r}')e^{jk\hat{\boldsymbol{k}}\cdot\boldsymbol{r}'}dS'\right], \quad (2)$$

where $k = 2\pi/\lambda$, λ is the wavelength and j is the imaginary unit, while the wave vector $\hat{\boldsymbol{k}} = \sin\theta\cos\phi\hat{\boldsymbol{x}} + \sin\theta\sin\phi\hat{\boldsymbol{y}} + \cos\theta\hat{\boldsymbol{z}}$ and the integration point is $\boldsymbol{r}' = x'\hat{\boldsymbol{x}} + y'\hat{\boldsymbol{y}} + z'\hat{\boldsymbol{z}}$.

Since (2) is evaluated for N_{obs} observation points, each requiring a summation over all N_{int} integration points, the complexity is $\mathcal{O}(N_{\text{obs}}N_{\text{int}})$. Since N_{obs} and N_{int} typically scale as $\mathcal{O}(f^2)$, the total scaling is $\mathcal{O}(f^4)$. The value of N_{obs}, as well as N_{int}, is governed by the largest value of $|\boldsymbol{r}'|$. While PO can be sped up using Graphics Processing Units [6], this does not reduce the scaling against the frequency, and thus for very large problems, another approach is necessary.

The Fast Physical Optics (Fast-PO) algorithm allows a significant reduction in the scaling by using a multi-level approach. First, we apply a grouping (such as an Octree [7]) of the integration points into boxes in a tree-like multi-level structure, where the diameter of the boxes increases as we go up in the tree. On the finest level, we compute the integral

$$\boldsymbol{V}(\theta,\phi) = \frac{e^{-jk|\boldsymbol{r}|}}{|\boldsymbol{r}|}\frac{jk\eta_0}{4\pi}\hat{\boldsymbol{k}}\times \left[\hat{\boldsymbol{k}} \times \iint \boldsymbol{J}_{\mathcal{S}}(\boldsymbol{v}')e^{jk\hat{\boldsymbol{k}}\cdot\boldsymbol{v}'}dS'\right], \quad (3)$$

where $\hat{\boldsymbol{k}}$ is a point on the unit sphere, and $\boldsymbol{v}'$ is the vector from the center of the group on the finest level to the integration point. Since $|\boldsymbol{v}'|$ is much smaller than $|\boldsymbol{r}'|$ in (2), we can settle for a much coarser sampling of the field, thereby reducing N_{obs} significantly. Having sampled $\boldsymbol{V}$ at a low number of output points, we can then apply interpolation to get the output at the original N_{obs} points, and subsequently restore the original phase. Thus, we can recover $\boldsymbol{E}_{\text{far}}$ using

$$\boldsymbol{E}_{\text{far}} = \iint e^{jk\hat{\boldsymbol{k}}\cdot(\boldsymbol{r}'-\boldsymbol{v}')}\mathcal{W}\left\{\boldsymbol{V}\right\}dS'. \quad (4)$$

Here, $\mathcal{W}$ is an interpolation operator in (θ, ϕ), usually based on low-order polynomials, which, along with restoration of the original phase using $e^{jk\hat{\boldsymbol{k}}\cdot(\boldsymbol{r}'-\boldsymbol{v}')}$, allows the required field to be computed much faster than by direct evaluation of (2). Since $\boldsymbol{V}$ varies much slower than $\boldsymbol{E}$ as a function of direction due to the fact that $|\boldsymbol{v}'| \ll |\boldsymbol{r}'|$, $\boldsymbol{V}$ is typically dubbed the *phase-compensated* field.

It is worth noting that in the work previously presented on far-field Fast-PO [5], [8], the accuracy has been fairly modest, with an error higher than 0.1% Relative RMS, which corresponds roughly to 1 dB deviation at 60 dB below peak. However, even 0.1% would generally be too large an error for use in reflector antenna problems, particularly in the final stages of a design. Further, the sampling rules presented in the literature require an oversampling parameter to account for inaccuracies in the interpolation procedure, and no exact rule exists for selecting this parameter to achieve a specified accuracy, which means that one cannot be sure that a specified accuracy has been achieved.

To overcome these challenges, we have improved the existing Fast-PO implementation for far-field problems, resulting in a significantly faster routine. In particular, this allows the combination of Fast-PO with the highly efficient PO integration rules used in TICRA's flagship product GRASP. Section III demonstrates the speed and accuracy relative to the direct PO in GRASP on a few examples.

B. Near-field PO

Calculating the magnetic field incident on a surface due to the surface current distribution on another surface constitutes the majority of the computational load in many PO tasks. The surface integral to be evaluated is of the form

$$\boldsymbol{H}_i(\boldsymbol{r}) = -\frac{1}{4\pi}\iint \left(\hat{\boldsymbol{R}} \times \boldsymbol{J}_{\mathcal{S}}(\boldsymbol{r}')\right) \cdot \frac{1+jk|\boldsymbol{R}|}{|\boldsymbol{R}|^2}e^{-jk|\boldsymbol{R}|}dS', \quad (5)$$

where $\boldsymbol{R} = \boldsymbol{r} - \boldsymbol{r}' = (x-x')\hat{\boldsymbol{x}} + (y-y')\hat{\boldsymbol{y}} + (z-z')\hat{\boldsymbol{z}}$ and $\boldsymbol{J}_{\mathcal{S}}$ is the surface current density on the illuminating object.

Since the Green's function now contains the norm of a vector, rather than the dot product between two vectors as was the case for the far-field integral (2), the phase-compensation used for the far-field problem is no longer sufficient. Using a multi-level grouping of the source points, [9], [10] have considered the use of a phase-and-amplitude compensated field using

$$\boldsymbol{V}(\boldsymbol{r}) = s(\boldsymbol{r},\boldsymbol{r}')e^{jks(\boldsymbol{r},\boldsymbol{r}')}\boldsymbol{H}_i(\boldsymbol{r}), \quad (6)$$

where

$$s(\boldsymbol{r},\boldsymbol{r}') = \sqrt{|\boldsymbol{r}-\boldsymbol{r}'_N|^2 + \frac{(D_N/2)^2}{2}} \quad (7)$$

in which $\boldsymbol{r}'_N$ is the center of the group in which the source point $\boldsymbol{r}'$ is located, and D_N is the diameter of that group at the level at which (6) is applied. With these compensations, the interpolation (which is performed both for the angular and the radial component, although [10] to some extent avoids the radial component by interpolating on the surface of the structure) becomes more manageable.

We stress that the accuracy of interpolation for near-field Fast-PO as presented in [9] will significantly depend upon the distance between the source and integration domains relative to the aperture of the source. In other words, the closer we move into the near-field, the more irregularly the field will behave (even with the phase-and-amplitude compensation), and thus the accuracy will suffer. This is treated in [9] by the introduction of a lower limit $\Omega_R > 1$, such that observation points that are located within the distance

$$\frac{D}{2}\Omega_R \quad (8)$$

from the center of the source points, with D being the diameter of the minimum sphere containing all source points, will be treated via direct application of (5). Again, choosing Ω_R along with the oversampling ratios to achieve a pre-specified upper bound on the error is not straight-forward. Further, we note that the limit in (8) depends linearly on D, while the region in which the near-field behaves irregularly depends quadratically on D, meaning that the errors as a function of Ω_R discussed in [9] will not necessarily be applicable for larger structures.

Our numerical experiments have revealed that even with specialized radial interpolation routines based on the near-field behaviour of an electromagnetic field [11, App. A], rather than simple polynomial interpolation, the interpolation becomes incontrollable as we move far inside the near-field of the radiating antenna. This does not lead to errors in using the Fast-PO as presented in the current literature, since it is handled by switching to direct integration, but it means that Fast-PO will not accelerate the computation. While this limitation on the distance between source and observation regions might be acceptable in some scenarios, e.g. in dual reflector systems for sub-to-main interactions where the main reflector is sometimes located outside the limit specified by (8), it renders the approach useless for e.g. main-to-sub interactions (such as computing the blockage by the subreflector). For other applications such as a Compact Antenna Test Range (CATR), where the sub- and main reflectors are often of comparable size and located quite close, the Fast-PO as presented in the literature is simply not applicable at all.

To overcome these bottlenecks, we have developed a new algorithm that combines the speed of FaFFA with the thorough sampling rules and phase-compensation of Fast-PO, resulting in superior accuracy and much lower runtimes, particularly for large problems, with the limitation on the distance between source and observation points being on the order of 1λ before switching to direct PO. Section III will demonstrate the performance for some practical scenarios.

III. Examples

In this section, we examine the accuracy and speed of the algorithms (near- and far-field) in comparison with regular PO.

The error is computed as the Relative RMS

$$\text{Relative RMS} = \sqrt{\frac{\sum_{i=1}^{N_s} |\boldsymbol{E}_{i,\text{direct}} - \boldsymbol{E}_{i,\text{fast}}|^2}{\sum_{i=1}^{N_s} |\boldsymbol{E}_{i,\text{direct}}|^2}}, \tag{9}$$

where $\boldsymbol{E}_{i,\text{direct}}$ and $\boldsymbol{E}_{i,\text{fast}}$ denote the direct PO (from (2) or (5)) and the Fast-PO electric field at the i^{th} sample point, respectively, and N_s is the number of samples. We stress that the reference field is not the true physical field, but rather the field as computed by direct integration of (2) or (5). As such, the accuracy is independent of e.g. the choice of integration rule for the surface integrals, since this rule is the same for direct PO and Fast-PO. Thus, the Relative RMS is only affected by the error made by applying Fast-PO instead of direct PO and consequently, in theory, a Relative RMS of 0 is possible if perfect interpolation were possible and no rounding errors were present.

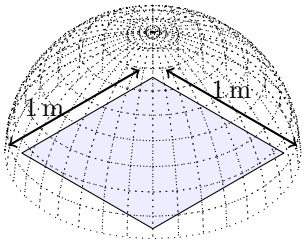

Fig. 1. Configuration for test case A.

A. Scattering by a plate

As an illustration of the performance of the algorithms for near- and far-field radiation on a simple geometry, we consider the scattering from a $1\,\text{m} \times 1\,\text{m}$ plate, illuminated by a plane wave at 45° incidence at varying frequencies. The configuration is illustrated in Figure 1.

For the near-field setup, we evaluate the field on a half-sphere, with a radius of $0.8\,\text{m}$ and origin at the center of the plate. The points are distributed equidistantly in a $\theta\phi$ grid, with the total number of points N_{obs} determined based on the wavelength λ (in metres) of the incident field, such that

$$N_{\text{obs}} = \frac{25}{\lambda^2}, \tag{10}$$

while the number of integration points is determined based on an auto-convergence procedure, requiring -80 dB accuracy [12]. The time required for auto-convergence is not included in the timings. We note that the observation sphere is located quite close to the plate, and with the frequency being varied between $12\,\text{GHz}$ and $192\,\text{GHz}$, the observation points are located deep within the reactive near-field region, typically taken to be the region for which $|\boldsymbol{R}| < 0.62\sqrt{D^3/\lambda}$ in (5).

By adjusting the frequency, we get the timings illustrated in Figure 2. The Relative RMS achieved varies slightly between the frequencies, but is far below the specified limit of 10^{-4}. Fitting a linear curve to the timings, we get close to the expected $\mathcal{O}(f^4)$ behaviour from the direct PO routine, while the Fast-PO timings scale slightly better than $\mathcal{O}(f^2)$. If we increased the frequency further, we would expect the scaling to eventually reach the $\mathcal{O}(f^2 \log f^2)$ scaling suggested in the literature.

For the far-field algorithm, we choose a very similar setup. The field is evaluated in a $\theta\phi$-grid with $\theta \in [-\pi/2, \pi/2]$, $\phi \in [0, 2\pi[$, and the number of points N_{obs} on the grid is chosen using (10) while the number of integration points are chosen using auto-convergence. We get the results illustrated in Figure 3. Once again, the Relative RMS achieved varies slightly between the frequencies, but is not above the limit 10^{-4}.

B. Torus

Another example is the torus antenna shown in Figure 4, designed by TICRA for a specific remote-sensing application

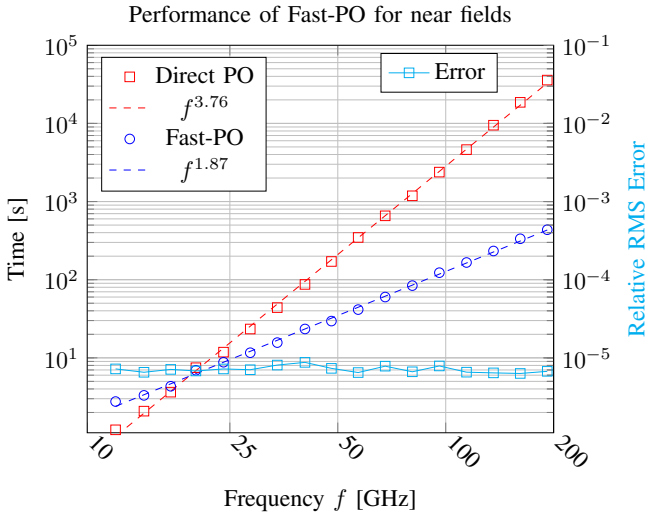

Fig. 2. Performance of our Fast-PO implementation for near fields compared to the direct PO implementation in GRASP 10.3. The Relative RMS Error between the fields obtained from direct PO and Fast-PO is shown in cyan.

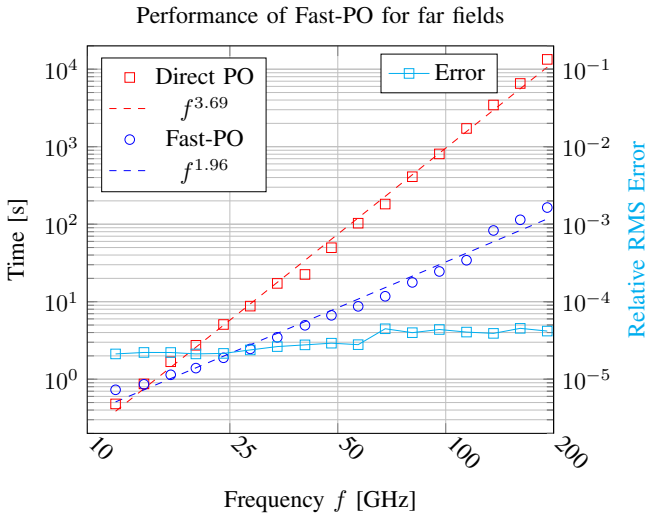

Fig. 3. Performance of our Fast-PO implementation for far fields compared to the direct PO implementation in GRASP 10.3. The Relative RMS Error between the fields obtained from direct PO and Fast-PO is shown in cyan.

[13]. It is generated by rotating a parabola around a tilted axis, and has the characteristics that it minimizes the scan loss for beams generated by feed elements located on a curve intersecting the focal point. It is important to evaluate the pattern from the antenna over a very large angular region since the application is a radiometer on a low-orbit satellite from which the earth subtends an angle of more than 60°.

The observation points are distributed in a 3201×3201 uv grid covering the region of earth visible from the satellite, yielding a total of $N_{\text{obs}} = 10246401$ far-field observation points.

We use the auto-convergence to determine the number of integration points on the surface, which yields $N_{\text{int}} = 607127$. We do not include PTD, since the auto-convergence finds that

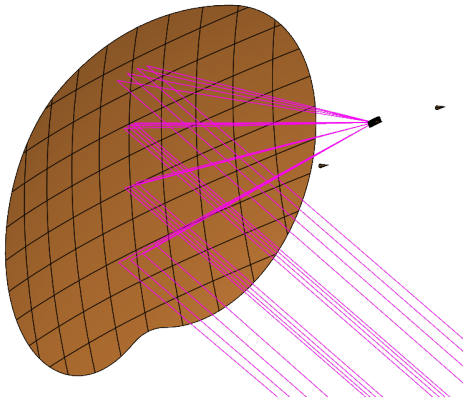

Fig. 4. Illustration of the geometry for the torus reflector.

the PTD contribution is not relevant at the specified (-80 dB) accuracy. This is due to the low edge illumination from the array. With GRASP 10.3, we find the solution in 1:27 H, while the Fast PO algorithm requires 4:33 minutes, a speedup of almost a factor of 20. The Relative RMS in the co-polar component is $2 \cdot 10^{-5}$, while in the cross-polar component it is slightly higher at $5 \cdot 10^{-5}$, both of which are significantly below the requested 10^{-4} error.

C. CATR

As a final example, we consider the compensated compact range from Airbus Defence & Space, the CCR 75/60, which was also investigated in [14]. The main reflector is 7.5 m times 6.0 m, resulting in a quiet zone (QZ) with a diameter of 5 m, in which the field has the same characteristics as a plane wave. The setup is illustrated in Figure 5. The simulation is carried out by applying the direct path through the system; the feed illuminates the subreflector, which in turn illuminates the main reflector, and the electric field from the main reflector is computed in the QZ. The vast majority of the computing time is spent on computing the illumination of the main reflector, due to the large amount of current points on both the sub- and main reflectors, including the serrations. In particular, the effects of the serrations as shown in Figure 6 are quite challenging to accurately model using PO, requiring a large number of current points. We note that the number of current points is again found using an auto-convergence procedure. We do not use PTD since its contribution in the QZ is very low.

The PO algorithm in GRASP 10.3 requires 3:30 hours to compute the interaction between the sub and main reflector at 6 GHz. Using Fast-PO, we tighten our requirements to the accuracy due to the highly sensitive application, requesting a relative error of 10^{-5}. The computation requires 1:20 minutes using Fast PO, resulting in a speed-up of a factor of 157 with a Relative RMS less than $4 \cdot 10^{-6}$. The performance in the QZ is illustrated in Figure 7 for an amplitude cut.

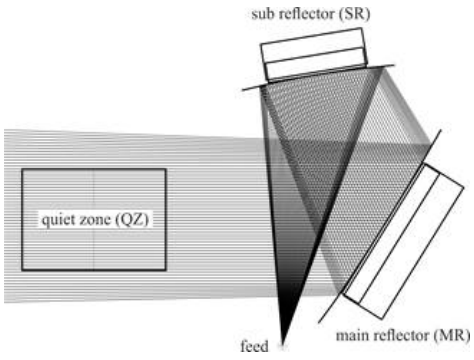

Fig. 5. Schematic of a compensated compact range.

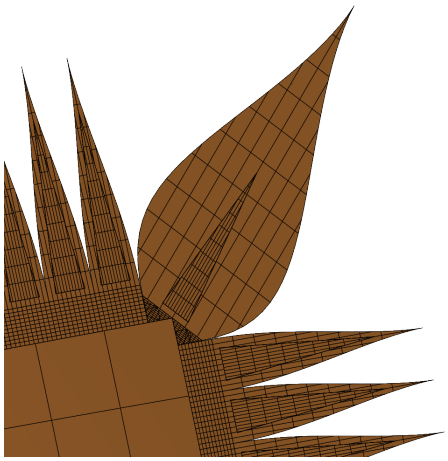

Fig. 6. A screenshot showing part of the model of the CATR reflector. Note the complicated shape of the serrations, particularly the corner serration, which makes the PO computation significantly more challenging.

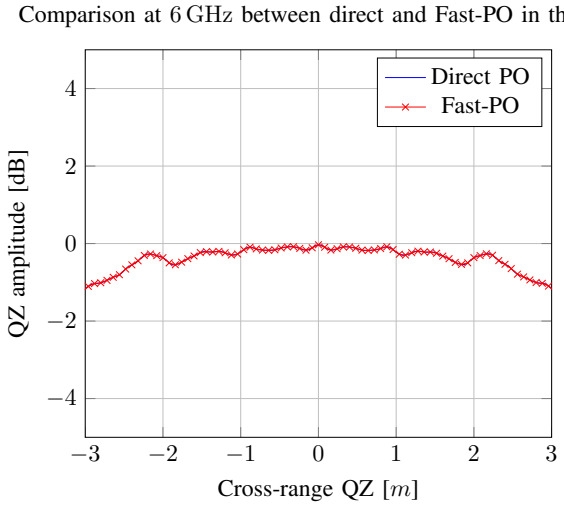

Fig. 7. A comparison between the results achieved by Direct PO and Fast PO in the quiet zone. With a Relative RMS less than $4 \cdot 10^{-6}$ in the range $[-8, 8]$ m, the results are indistinguishable, particularly in the center of the quiet zone as illustrated here.

IV. Conclusion

The examples show that our implementation of accelerated Physical Optics (Fast-PO), involving more efficient interpolation for the far field Fast-PO and a new approach for near field Fast-PO, provides extreme speedups while maintaining the very low error level required for the final stages of a design. Details of the algorithm, including the implementation of the Physical Theory of Diffraction (PTD) contribution into the acceleration scheme, are still under development. However, the performance of the current algorithm allows a reduction in time by a factor of 10 to 100, depending on the application. For a practical application involving the design of a Compact Antenna Test Range, Fast-PO offers a reduction in time from 3.5 hours to 1:20 minutes, thus facilitating a much more efficient design process and even opening up the possibility of allowing small-scale optimization.

References

[1] C.-C. Lu and W. C. Chew, "Fast far-field approximation for calculating the RCS of large objects," *Microwave and Optical Technology Letters*, vol. 8, no. 5, pp. 238–241, Apr. 1995.

[2] E. Michielssen and A. Boag, "Multilevel evaluation of electromagnetic fields for the rapid solution of scattering problems," *Microwave and Optical Technology Letters*, vol. 7, no. 17, pp. 790–795, 1994.

[3] A. Boag, "A fast iterative physical optics (FIPO) algorithm based on non-uniform polar grid interpolation," *Microwave and Optical Technology Letters*, vol. 35, no. 3, pp. 240–244, 2002.

[4] A. Boag and E. Michielssen, "A Fast Physical Optics (FPO) Algorithm for Double-Bounce Scattering," *IEEE Transactions on Antennas and Propagation*, vol. 52, no. 1, pp. 205–212, Jan. 2004.

[5] A. Boag, "A Fast Physical Optics (FPO) Algorithm for High Frequency Scattering," *IEEE Transactions on Antennas and Propagation*, vol. 52, no. 1, pp. 197–204, Jan. 2004.

[6] O. Borries, H.-H. B. Sørensen, B. Dammann, E. Jørgensen, P. Meincke, S. B. Sørensen, and P. C. Hansen, "Reflector Antenna Analysis using Physical Optics on Graphics Processing Units," in *European Conference on Antennas and Propagation*, Apr. 2014.

[7] D. Meagher, "Geometric modeling using octree encoding," *Computer Graphics and Image Processing*, vol. 19, no. 2, pp. 129–147, Jun. 1982.

[8] A. Manyas and L. Gürel, "Memory-Efficient Multilevel Physical Optics Algorithm for Fast Computation of Scattering From Three-Dimensional Complex Targets," in *Computational Electromagnetics International Workshop*. IEEE, 2007, pp. 26–30.

[9] Y. Brick and A. Boag, "Multilevel Nonuniform Grid Algorithm for Acceleration of Integral Equation-Based Solvers for Acoustic Scattering," *IEEE Transactions on Ultrasonics, Ferroelectrics and Frequency Control*, vol. 57, no. 1, pp. 262–273, Jan. 2010.

[10] C. Letrou and A. Boag, "Near-field multilevel physical optics for fast analysis of multi-reflector antennas," *International Seminar Day on Diffraction Millennium Workshop*, 2013.

[11] J. Hansen, J. Hald, F. Jensen, and F. Holm Larsen, *Spherical Near-Field Antenna Measurements*, J. Hansen, Ed. London: Peter Peregrinus Ltd., 1988.

[12] K. Pontoppidan, *GRASP Technical Description*. TICRA, Mar. 2008.

[13] C. Cappellin, K. Pontoppidan, P. H. Nielsen, N. Skou, S. S. Søbjærg, M. Ivashina, O. Iupikov, A. Ihle, D. Hartmann, and K. van 't Klooster, "Novel multi-beam radiometers for accurate ocean surveillance," in *European Conference on Antennas and Propagation*, 2014, pp. 3531–3535.

[14] C. H. Schmidt, A. Geise, J. Migl, H.-J. Steiner, and H.-H. Viskum, "A Detailed PO/PTD GRASP Simulation Model for Compensated Compact Range Analysis with Arbitrarily Shaped Serrations," in *35th Antenna Measurement Techniques Association Conference Proceedings, AMTA, Columbus, Ohio*, 2013, pp. 6–11.